Acta Crystallographica Section A
Foundations of Crystallography
ISSN 0108-7673

Received 10 March 2000
Accepted 14 August 2000

A geometric centroid principle and its application

F. Mädler,[a]* E. Behrends[b] and K. Knorr[c]

[a]Hahn-Meitner-Institute Berlin, D-14109 Berlin, Germany, [b]Freie Universität Berlin, Institute for Mathematics I, D-14195 Berlin, Germany, and [c]Christian Albrechts University, Institute of Earth Sciences-Mineralogy, D-24098 Kiel, Germany. Correspondence e-mail: maedler@hmi.de

A new concept of approximation for rigid point sets is suggested. As a necessary condition of optimality, the principle of the conjoint centroid is proved: to achieve a best approximation, certain co-sets must conjoin their centroids. The practical use of the centroid principle, and how it opens up a non-classical method of modelling various aspects of orientational disorder in crystals, is demonstrated. The principle is applied to the interpretation of density data, to the prediction of high-pressure conformations through qualitative simulations, and to the prediction and computation of disordered sets of possible reorientation pathways which explain the shape of the electron-density distribution reconstructed from diffraction experiments. It is also demonstrated how an inversion of the centroid principle can be used to model forces between the parts of the disordered structures.

1. Motivation

Diffraction experiments are an important and widely accepted means for the investigation of matter. However, they exhibit an inherent severe limitation: they can only provide the space-and-time average of the crystal structure, and it may be difficult to resolve the disorder of structural fragments like complex anions or molecules inside the crystal. To explain the static or dynamic ambiguity, the fragment may be embedded into density data such as electron density, scattering-length distribution *etc.* which are reconstructed from the scattering data (Knorr *et al.*, 1998). In general, the embedding is a non-differentiable complex problem. We will show that the necessity for a conjoint geometric centroid for the disordered object and for the non-disordered part of the crystal opens up a non-classical way of embedding the structural fragment into density data in full orientational disorder by means of gradient-free methods (Knorr & Mädler, 1999). In this sense, the principle of the conjoint centroid is an important step towards an implicit computer-based model of disorder in crystals, which represents static or dynamic ambiguity in the form of solutions to suitable optimization problems. Up to a certain degree, such a qualitative model – which uses geometric instead of physical concepts – can compensate for the lack of explicit quantitative formulae.

In §2, the basic version of the principle is proved and the question of sufficiency is discussed. A more elaborated version, which better meets the demands of practical applications, is stated in §3, together with some more general aspects of its applicability. In §4, computational aspects are discussed. Finally, in §5, we briefly report on several crystallographic problems and show how the centroid principle facilitates their solution.

2. The principle of the conjoint centroid

There is a well known minimum property of the triangle's centroid:[1] it is the unique point that minimizes the sum of its squared distances from the vertices. It seems to be less known that every finite subset of the Euclidean space $\Re^n$ has this minimum property. To give an example, for every point of the plane background in Fig. 1, its colour indicates the squared and summed distances of this point from the red points of the set $\mathcal{M}$. It follows from the lemma (see §2.1) that the blue centroid $\mathcal{C}$ of $\mathcal{M}$ must be the bright centre in the background.

We may look at the centroid's minimum property from a different point of view: for a triangle $\mathcal{F}$ and a fixed point Y somewhere in space, we can look for best approximations to Y by the triangle. Of course, any position $\mathcal{F} = (X_1, X_2, X_3)$, the centroid $\overline{\mathcal{F}} := (X_1 + X_2 + X_3)/3$ of which satisfies $\overline{\mathcal{F}} = Y = \overline{Y}$, is an answer to this problem. It seems to be widely unknown that this necessity for identical centroids can be generalized to partitions of finite point sets. If the parts are 'rigid fragments' in the sense that their mobility is restricted to isometric mappings, loosely verbalized our central theorem states (theorem 1, §2.3): rigid point sets which mesh one another in a best approximation must have a conjoint centroid.

Let $X = (x_j)_{j=1}^n$ be points in the Euclidean space $\Re^n$, with the inner product (*e.g.* Valenza, 1993)

[1] Centroid, median point, centre of mass, centre of gravity, centre of attraction, expectation, first-order momentum and spatial mean: all these notions in one way or the other deal with the same point $\overline{\mathcal{F}}$ which, in the case of the triangle, $\mathcal{F} = (X_1, X_2, X_3)$, is the spatial average of the vertices, *i.e.* $\overline{\mathcal{F}} = (X_1 + X_2 + X_3)/3$ (*e.g.* Weisstein, 1999). Here we use 'centroid' since we would like to strip the notion of the additional meanings it carries in physics or statistics, thus emphasizing its purely geometric aspects.

$$\langle X, Y\rangle := \sum_{j=1}^{n} x_j y_j$$

and the norm

$$\|X\| := \langle X, X\rangle^{1/2}.$$

For translations A of $\Re^n$, orthogonal $n \times n$ transformations U and a collection of points $X_1, \ldots, X_N \in \Re^n$, we consider isometric images X_i' of the points X_i, *i.e.*

$$X_i' := UX_i + A, \quad i = 1, \ldots, N.$$

For a fixed collection of points $Y_1, \ldots, Y_N \in \Re^n$, their approximation by these images is measured by means of a weighted residual,

$$R(A, U) := \sum_{i=1}^{N} p_i \|Y_i - (UX_i + A)\|^2,$$

with weights

$$p_i > 0, \quad \sum_{i=1}^{N} p_i = 1.$$

Note that the points $X_1, \ldots, X_N, Y_1, \ldots, Y_N$ are not requested to be pairwise different. In the first part of this section, we prove the centroid principle to be a necessary condition for an optimal isometric mapping $(A^\star, U^\star)$; in particular, we determine the optimal translation $A = A^\star$ which minimizes the residual

$$R(A) = \sum_{i=1}^{N} p_i \|Y_i - (W_i + A)\|^2$$

for a fixed set of arbitrary points $W_i \in \Re^n$ (including the case $W_i := U^\star X_i$) and reveal the relation between $A^\star$ and the weighted centroids of the points involved (theorem 1, §2.3). In the second part, a necessary and sufficient condition for optimal transformations $U^\star$ is derived (theorem 2, §2.5), and from that a sufficient condition for minimizing transformations $U^\star$ for dimension $n = 2$, *i.e.* for rotations $[\det(U) = 1]$ or roto-inversions $[\det(U) = -1]$ (theorem 3, §2.6). For $n \geq 3$, we suggest the use of Monte Carlo methods and evolution strategies for the computation of the images $U^\star X_1, \ldots, U^\star X_N$ which minimize the residual $R(U)$.

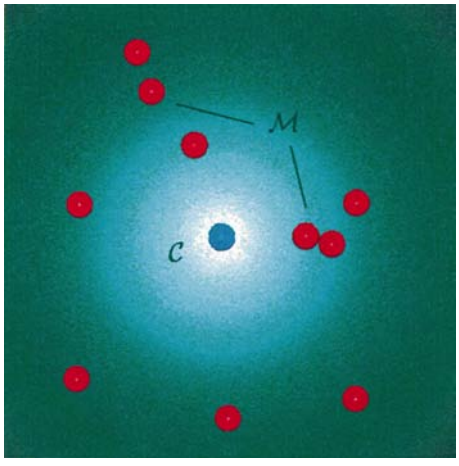

Figure 1
Visualizing the centroid's minimum property for a set $\mathcal{M}$ of random points Z_i: the blue centroid $\mathcal{C}$ of $\mathcal{M}$ is the unique minimum of the function $F(A) := (1/N)\sum_{i=1}^{N} \|Z_i - A\|^2$, $A \in \Re^3$.

2.1. Lemma

Let the points $Z_1, \ldots, Z_N \in \Re^n$ have their weighted centroid at the origin,

$$\sum_{i=1}^{N} p_i Z_i = \mathcal{O}, \quad p_i > 0, \quad \sum_{i=1}^{N} p_i = 1.$$

Then, for every translation $A \in \Re^n$, the equation

$$\sum_{i=1}^{N} p_i \|Z_i - A\|^2 = \sum_{i=1}^{N} p_i \|Z_i\|^2 + \|A\|^2 \qquad (1)$$

holds. Furthermore, the unique minimum of the function

$$F(A) = \sum_{i=1}^{N} p_i \|Z_i - A\|^2$$

is the origin $A = \mathcal{O}$.

2.2. Proof

To prove equation (1), we use the special form of the Euclidean norm which is induced by an inner product,

$$\begin{aligned}\sum p_i \|Z_i - A\|^2 &= \sum p_i \langle Z_i - A, Z_i - A\rangle \\ &= \sum p_i \|Z_i\|^2 + \sum p_i \|A\|^2 - 2\sum p_i \langle Z_i, A\rangle \\ &= \sum p_i \|Z_i\|^2 + \|A\|^2 - 2\Big\langle \sum p_i Z_i, A\Big\rangle \\ &= \sum p_i \|Z_i\|^2 + \|A\|^2.\end{aligned}$$

Now, $F(A)$ is represented by the right-hand side of equation (1) which is minimal if and only if $A = \mathcal{O}$.

To give an interpretation of the lemma, we show that it contains a proof of the centroid's minimum property which we started from at the beginning of this section and which is illustrated in Fig. 1 (for a set $\mathcal{M}$ of N different points Z_i and equal weights $p_i = 1/N$): if we assume (without loss of generality) that the centroid $\mathcal{C} = (\sum Z_i)/N$ of $\mathcal{M}$ coincides with the origin $\mathcal{O}$, then, according to the lemma, the centroid uniquely minimizes the function $F(A)$, and hence the function

$$NF(A) = \sum_{i=1}^{N} \|Z_i - A\|^2,$$

i.e. the centroid uniquely minimizes the squared and summed distances as mentioned above.

The following theorem generalizes the issue.

2.3. Theorem 1 – principle of the conjoint centroid

Let $Y_1, \ldots, Y_N \in \Re^n$ denote a fixed collection of points and $W_1, \ldots, W_N$ denote a second collection which is mapped by translations $A \in \Re^n$, with the weighted residual

$$R(A) = \sum_{i=1}^{N} p_i \|Y_i - (W_i + A)\|^2.$$

If $A = A^\star$ is selected such that the residual is minimal,

$$R(A^\star) = \min_{A\in\Re^n} R(A)$$

then the weighted centroids are identical,

$$\sum_{i=1}^{N} p_i Y_i = \sum_{i=1}^{N} p_i (W_i + A^\star)$$

and $A^\star = \sum p_i (Y_i - W_i)$ is the unique minimum of the residual $R(A)$.

2.4. Proof

Let

$$A_0 := \sum_{i=1}^{N} p_i (Y_i - W_i).$$

Since this identity can be rewritten in the form $\sum p_i Y_i = \sum p_i (W_i + A_0)$, the proof is complete once we have shown that A_0 uniquely minimizes the residual R.

In order to apply the above lemma to the points

$$Z_i := Y_i - (W_i + A_0), \quad i = 1, \ldots, N,$$

we have to show that their weighted centroid coincides with the origin $\mathcal{O} \in \Re^n$,

$$\begin{aligned}\sum p_i Z_i &= \sum p_i (Y_i - W_i - A_0) \\ &= \sum p_i (Y_i - W_i) - A_0 \sum p_i \\ &= A_0 - A_0 = \mathcal{O}.\end{aligned}$$

For a minimizing translation $A^\star$ select A_1 such that $A^\star = A_0 + A_1$. Then, for the minimum value of the residual we have

$$\begin{aligned}R(A^\star) &= \sum p_i \| Y_i - (W_i + A^\star) \| \\ &= \sum p_i \| [Y_i - (W_i + A_0)] - A_1 \|.\end{aligned}$$

From the lemma we conclude $A_1 = \mathcal{O}$; hence, $A^\star = A_0$ is the unique minimum of R. This completes the proof.

Since the theorem includes the case $W_i := U^\star X_i$, it provides a sound and effective way to facilitate the best approximation of points $Y_1, \ldots, Y_N$ by isometric images $X'_1, \ldots, X'_N$ of points $X_1, \ldots, X_N$: settle the translation part first [which means a shift $T = \sum p_i (Y_i - X_i)$ to the weighted centroid of the differences], then look for optimal transformations $U^\star$. For the sequel, without loss of generality, we assume that the point collections $X_1, \ldots, X_N$ and $Y_1, \ldots, Y_N$ have their conjoint centroid at the origin $\mathcal{O}$ of the space $\Re^n$.

In order to derive a condition for optimal transformations[2] $U^\star$, consider the residual

$$R(U) = \sum_{i=1}^{N} p_i \| Y_i - U X_i \|^2. \tag{2}$$

For every orthogonal (hence length-preserving) transformation U, the residual can be rewritten

$$\begin{aligned}R(U) &= \sum p_i \langle Y_i - UX_i, Y_i - UX_i \rangle \\ &= \sum p_i (\|Y_i\|^2 + \|X_i\|^2) - 2 \sum p_i \langle Y_i, UX_i \rangle.\end{aligned}$$

Obviously $R(U)$ is minimal if and only if the subtracted term on the right is maximal, *i.e.* if the images UX_i are 'as parallel as possible' to the vectors Y_i which they approximate. This provides a necessary and sufficient condition for optimal transformations $U^\star$.

2.5. Theorem 2 – characterization of optimal $U^\star$

An orthogonal transformation $U^\star$ minimizes the residual

$$R(U) = \sum_{i=1}^{N} p_i \| Y_i - U X_i \|^2 \tag{3}$$

if and only if it maximizes the function

$$G(U) := \sum_{i=1}^{N} p_i \langle Y_i, UX_i \rangle. \tag{4}$$

In the case of two dimensions, for every orthogonal matrix U there exists an angle φ and a pair of opposite signs $s_1, s_2 \in \{1, -1\}$ such that $G = G(U(\varphi, s_1, s_2))$ has the representation

$$\sum_{i=1}^{N} p_i \left\langle \begin{pmatrix} y_1^{(i)} \\ y_2^{(i)} \end{pmatrix}, \begin{pmatrix} \cos\varphi & s_1 \sin\varphi \\ \sin\varphi & s_2 \cos\varphi \end{pmatrix} \begin{pmatrix} x_1^{(i)} \\ x_2^{(i)} \end{pmatrix} \right\rangle.$$

Evaluation of the inner products shows that G can be expressed as a function of φ,

$$g(\varphi) := c_1 \sin\varphi + c_2 \cos\varphi, \tag{5}$$

with coefficients $c_1 = c_1(s_1)$ and $c_2 = c_2(s_2)$,

$$\begin{aligned}c_1 &= \sum_{i=1}^{N} p_i [x_1^{(i)} y_2^{(i)} + s_1 x_2^{(i)} y_1^{(i)}] \\ c_2 &= \sum_{i=1}^{N} p_i [x_1^{(i)} y_1^{(i)} + s_2 x_2^{(i)} y_2^{(i)}].\end{aligned} \tag{6}$$

Differentiation of g with respect to φ yields

$$g'(\varphi) = c_1 \cos\varphi - c_2 \sin\varphi.$$

In the cases $c_2 \neq 0$, the optimal angles $\varphi^\star$ are among the solutions to the equation

$$\tan\varphi = c_1 / c_2.$$

Then, for suitable integers k_0 and $k_0 + 1$, two different solutions $\varphi_{1,2}$ for

$$\varphi = \arctan(c_1/c_2) + k\pi, \quad k \in \mathbb{Z},$$

belong to the interval $[0, 2\pi)$. Since, in this case, the second derivative of g is $-g$, the solution $\varphi^\star$ with $g(\varphi^\star) > 0$ is the angle which maximizes g; its orthogonal matrix $U^\star = U(\varphi^\star, s_1, s_2)$ maximizes the function G and minimizes the residual R. Note that both sign pairs $[s_1^{(j)}, s_2^{(j)}]$ have to be tested in order to decide whether rotation or roto-inversion (or both) leads to the global optimum $U^\star$.

This result is summarized in the following theorem.

[2] Because of compactness, an optimal $U^\star$ always exists: the set of orthogonal transformations is bounded and closed in a finite-dimensional space, and the residual (2) is continuous.

2.6. Theorem 3 – sufficiency of $U^\star$ for dimension $n = 2$

Let the point collections $Y_1, \ldots, Y_N$ and $X_1, \ldots, X_N$ have their conjoint centroid at the origin $\mathcal{O} \in \Re^2$. For rotation ($s_1 = -1$ and $s_2 = 1$) or roto-inversion ($s_1 = 1$ and $s_2 = -1$) let the coefficients $c_2^{(1)}, c_2^{(2)}$ hold,

$$c_2^{(j)}(s_2^{(j)}) = \sum_{i=1}^{N} p_i [x_1^{(i)} y_1^{(i)} + s_2^{(j)} x_2^{(i)} y_2^{(i)}] \neq 0$$

for $j = 1, 2$. Then there is a unique rotation

$$U^\star = U^\star(\varphi^{(1)}, s_1^{(1)}, s_2^{(1)})$$

or a unique roto-inversion

$$U^\star = U^\star(\varphi^{(2)}, s_1^{(2)}, s_2^{(2)})$$

which maximizes the function

$$G(U) = \sum_{i=1}^{N} p_i \langle Y_i, UX_i \rangle.$$

Furthermore, with a suitable integer k_0, the optimal angle $\varphi^\star \in [0, 2\pi)$, which generates the optimal transformation $U^\star(\varphi^\star, s_1^{(j)}, s_2^{(j)})$, is given by the two equations

$$\varphi^{(j)} = \arctan[c_1^{(j)}/c_2^{(j)}] + k\pi, \quad k \in \mathbb{Z}, \quad j = 1, 2.$$

Note that theorem 3 does not provide a necessary optimality condition; for general point collections, uniqueness of the best transformation $U^\star$ cannot be expected. To give an example: for a triangle $\mathcal{F} = (X_1, X_2, X_3)$ spinning around its centroid

$$Y := (X_1 + X_2 + X_3)/3 = \mathcal{O},$$

we have $G \equiv 0$, and the minimum value of the residual

$$R(U(\varphi)) = \left(\|X_1\|^2 + \|X_2\|^2 + \|X_3\|^2\right)/3$$

does not depend on the angle φ. Equivalently, a closer look at the coefficients (6) shows that every term in the sums is multiplied by a zero component of Y, *i.e.* for all coefficients we have $c_r^{(j)} = 0$ ($r, j = 1, 2$), hence $g' \equiv 0$. We point out that this example is just a simple representative of a special class of residuals which is investigated in the following section (*cf.* example 1; §3.2).

For dimension $n = 3$, every orthogonal transformation U can be represented by suitable products of matrices (*e.g.* Giacovazzo, 1994):

$$U_x(\varphi_1) = \begin{pmatrix} s_1 & 0 & 0 \\ 0 & \cos\varphi_1 & -\sin\varphi_1 \\ 0 & \sin\varphi_1 & \cos\varphi_1 \end{pmatrix}$$

$$U_y(\varphi_2) = \begin{pmatrix} \cos\varphi_2 & 0 & \sin\varphi_2 \\ 0 & s_2 & 0 \\ -\sin\varphi_2 & 0 & \cos\varphi_2 \end{pmatrix} \qquad (7)$$

$$U_z(\varphi_3) = \begin{pmatrix} \cos\varphi_3 & -\sin\varphi_3 & 0 \\ \sin\varphi_3 & \cos\varphi_3 & 0 \\ 0 & 0 & s_3 \end{pmatrix}.$$

The integers s_i indicate rotation ($s_i = 1$) or roto-inversion ($s_i = -1$, $i = 1, 2, 3$), the subscripts x, y, z refer to the axis of the rotation. If the Eulerian angles $\theta_1, \theta_2, \theta_3$ are used, every orthogonal U is a product,

$$U = U_{z''}(\theta_3) U_{x'}(\theta_2) U_z(\theta_1),$$

where the subscript primes refer to transformed coordinates. With this representation of U, we could, in principle, evaluate the inner products of the function $G(U(\theta_1, \theta_2, \theta_3))$ as before [*cf.* equation (4)] and derive a function $g(\theta_1, \theta_2, \theta_3)$ which would have to be maximized. However, here and now, the sufficiency condition for optimal angles would involve the solution of a non-linear trigonometric system of equations

$$\frac{\partial}{\partial\theta_j} g(\theta_1, \theta_2, \theta_3) = 0, \quad j = 1, 2, 3,$$

which no longer has an explicit solution and must be solved approximately. Instead, for $n \geq 3$, we suggest the use of stable and robust Monte Carlo methods or evolutionary algorithms (*e.g.* Bäck, 1996) for a direct computation of the optimal images $X_1^\star, \ldots, X_N^\star$ for the residual (3) or the function (4). Since, by virtue of the centroid principle, translation is no longer part of the optimization, such methods are well suited for this less complex task. §§4 and 5 are dedicated to the details.

3. The concept of informed co-sets

Theorem 1 states the centroid principle in a very condensed form. At the same time, it provides a sound mathematical framework which we will now use to derive a more detailed and more flexible version of the principle that better meets the needs of specific applications; more detailed in the sense that it takes into account more complex relations between the point sets, *i.e.* their 'spatial mesh', and more flexible in that it is able to take up information about these relations that may depend on the particular application. We would like the principle to offer an interface to expert knowledge about predominant pairs of points that govern the 'interactions' of the point sets. In this section, we discuss the necessity for such an extension, prove the extended version of the principle and demonstrate its use along some simple examples.

To be able to describe a spatial mesh between the point sets, an extended version of the centroid principle must explicitly deal with those cases in which a point X_i of a set $\mathcal{F} = \{X_1, \ldots, X_N\}$ is related to more than one point Y_j of a set $\mathcal{P} = \{Y_1, \ldots, Y_M\}$, and *vice versa*. In Fig. 2(*a*), the dumbbell $\mathcal{F} = \{X_1, X_2\}$ and the black triangle $\mathcal{P} = \{Y_1, Y_2, Y_3\}$ can only be considered 'close' to each other if at least the three distances

$$R(\mathcal{F}) = \|Y_1 - X_1\|^2 + \|Y_3 - X_1\|^2 + \|Y_2 - X_2\|^2$$

contribute to the residual R, *i.e.* only if the point X_1 enters R twice. Without the term $\|Y_3 - X_1\|^2$, for instance, the influence of Y_3 on the approximation is lost, and 'close' would mean a collinear alignment of the two dumbbells $\mathcal{F}$ and $\{Y_1, Y_2\} \subset \mathcal{P}$.

Therefore, we extend the set $\mathcal{F} = \{X_1, X_2\}$ to its linearily ordered informed co-set $\mathcal{F}_\rho = (X_1, X_1, X_2)$ and take

$\mathcal{P}_\rho = (Y_1, Y_3, Y_2)$ as an informed co-set of $\mathcal{P}$. The subscript ρ indicates the relation

$$\rho = \{(X_1, Y_1), (X_1, Y_3), (X_2, Y_2)\}$$

of pre-selected point pairs which we want to contribute to the extended residual

$$R_\rho(\mathcal{F}) = \|\mathcal{P}_\rho - \mathcal{F}_\rho\|^2 = \sum_{i=1}^{3} \|Y_i - X_i\|^2$$

(where we have re-indexed the summation). After the extension, the complete information for a spatial mesh between $\mathcal{F}$ and $\mathcal{P}$ is stored in the informed pair $(\mathcal{F}_\rho, \mathcal{P}_\rho)$ of linearly ordered co-sets. In essence, this concept serves as an adequate vehicle to make a pre-selected mesh of the point sets $\mathcal{P}$ and $\mathcal{F}$ into a mesh of $\mathcal{P}$ and its best approximations $\mathcal{F}^\star$.

Note that, in general, the residual R_ρ may have multiple entries from both $\mathcal{F}$ and $\mathcal{P}$ at the same time. As will be shown now, the extended centroid principle holds for any relation $\rho \subseteq \mathcal{F} \times \mathcal{P}$ of the Cartesian product of the point sets. Of course, not all possible choices of ρ will be of equal interest in a particular application. Then expert knowledge can be used, interactively or stored in a knowledge base, to define appropriate residuals R_ρ that meet the specific needs of an application. This will become clearer from the examples of this section.

To treat the general case, let $\mathcal{P} = \{Y_1, \ldots, Y_M\}$ denote a fixed set of (pairwise different) points of $\Re^n$, and let

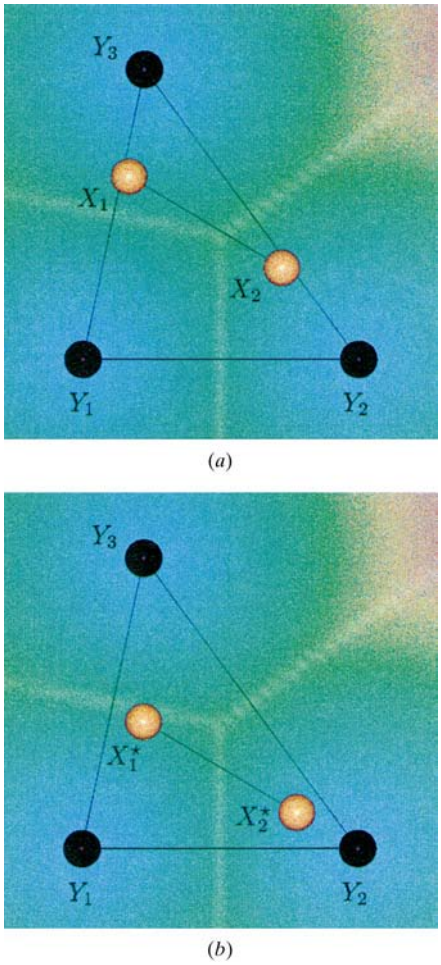

Figure 2
In (*a*) the dumbbell $\mathcal{F} = \{X_1, X_2\}$ is in a 'good' approximation with the triangle $\mathcal{P} = \{Y_1, Y_2, Y_3\}$. To capture the best approximation $\mathcal{F}^\star = \{X_1^\star, X_2^\star\}$ depicted in (*b*), the two points of $\mathcal{F}$ must mesh with all points of $\mathcal{P}$.

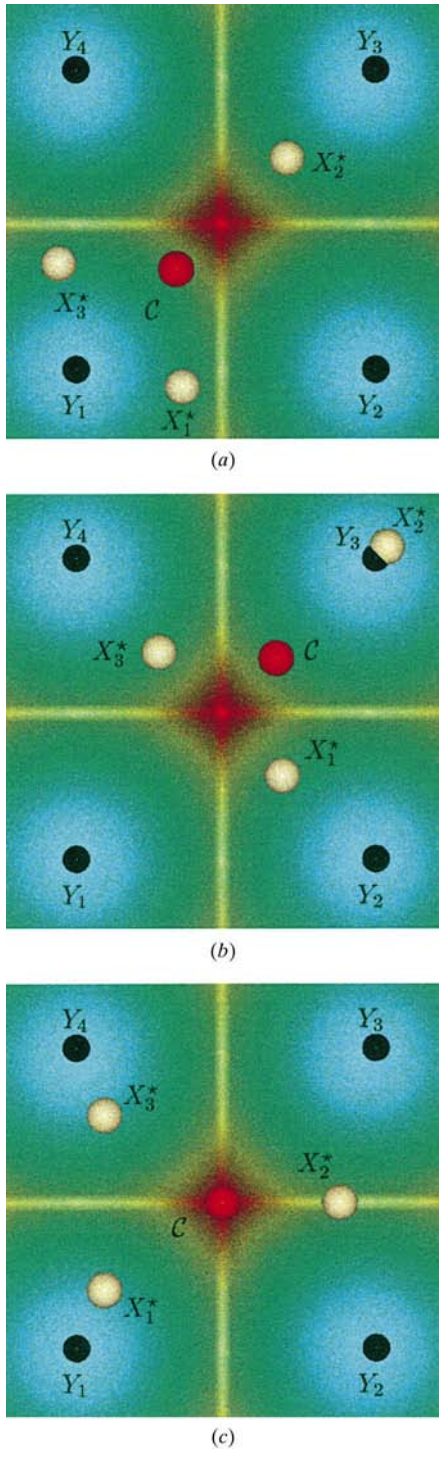

Figure 3
Three of the best short-range approximations of an isosceles triangle $\mathcal{F}^\star$ to a square $\mathcal{P} = \{Y_1, \ldots, Y_4\}$ (see text). Voronoi's cells help to identify appropriate approximation residuals. Symmetry facilitates the search for optimal solutions.

$\mathcal{F} = \{X_1, \ldots, X_N\}$ denote a second such set which may be subjected to translations $A \in \Re^n$. For a pre-selected relation $\rho \subseteq \mathcal{F} \times \mathcal{P}$, let the pairs $(X_i, Y_j) \in \rho$ be linearly ordered in the form

$$(X_i, Y_{i1}), \ldots, (X_i, Y_{in_i}), \quad i = 1, \ldots, N_\rho, \tag{8}$$

where $1 \leq N_\rho \leq N$. Then, in this order, we take the first entries to define the informed co-set

$$\mathcal{F}_\rho := (X_1, \ldots, X_L)$$

of $\mathcal{F}$, and the second entries to build the co-set

$$\mathcal{P}_\rho := (Y_1, \ldots, Y_L)$$

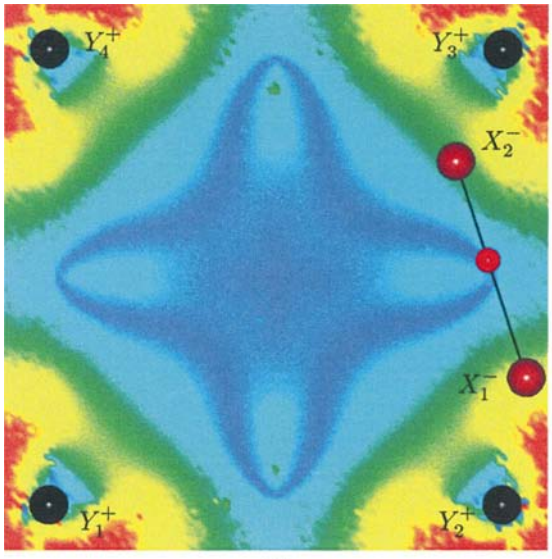

(*a*)

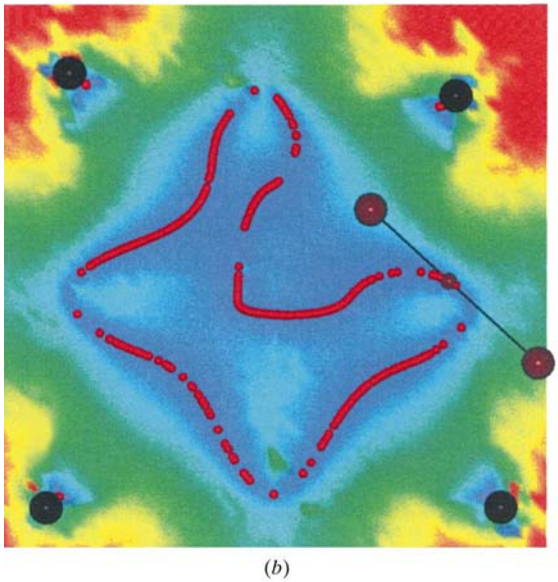

(*b*)

Figure 4
Coulomb equilibrium inside a fictitious ionic crystal. In (*a*), the conjoint centroids of the fragment $\mathcal{F} = (X_1^-, X_2^-)$ and the cell $\mathcal{P} = (Y_1^+, \ldots, Y_4^+)$ are located on the dark-blue star. In (*b*), the square is slightly distorted. The red balls indicate conjoint centroids as computed by a combined Monte Carlo and evolution strategy.

of $\mathcal{P}$, with

$$L := \sum_{i=1}^{N_\rho} n_i \leq NM.$$

Since the linear order (8) is compatible with translations, *i.e.*

$$(A + \mathcal{F})_\rho = (A + X_1, \ldots, A + X_N)_\rho = A + \mathcal{F}_\rho,$$

the weighted residual

$$R_\rho(A) := \sum_{i=1}^{L} p_i \|Y_i - (A + X_i)\|^2 \tag{9}$$

is well defined for any translation A. In total, the co-sets $\mathcal{F}_\rho, \mathcal{P}_\rho$ and their residual R_ρ satisfy the assumptions of theorem 1 so that the following corollary holds.

3.1. Corollary 1 – a structured form of the centroid principle

Let $\mathcal{P} = \{Y_1, \ldots, Y_M\} \subset \Re^n$ denote a fixed set of (pairwise different) points, and let $\mathcal{F} = \{X_1, \ldots, X_N\}$ denote a second such set which is mapped by translations $A \in \Re^n$. For a pre-selected relation $\rho \subseteq \mathcal{F} \times \mathcal{P}$, let $R_\rho(A)$ denote its weighted residual (9). Then, if $A = A^\star$ is selected such that $R_\rho(A^\star)$ is minimal, the informed co-sets $\mathcal{P}_\rho$ and $(A^\star + \mathcal{F})_\rho = A^\star + \mathcal{F}_\rho$ must have a conjoint weighted centroid

$$\sum_{i=1}^{L} p_i Y_i = \sum_{i=1}^{L} p_i (A^\star + X_i).$$

To demonstrate the use of the principle and the benefit from the informed co-sets, three rather different aspects of the principle are discussed along with some examples.

3.2. Example 1 – Cartesian residual

As a first example, we consider the Cartesian residual $R_{\mathcal{F}\times\mathcal{P}}$, which is defined by the Cartesian product of the point sets

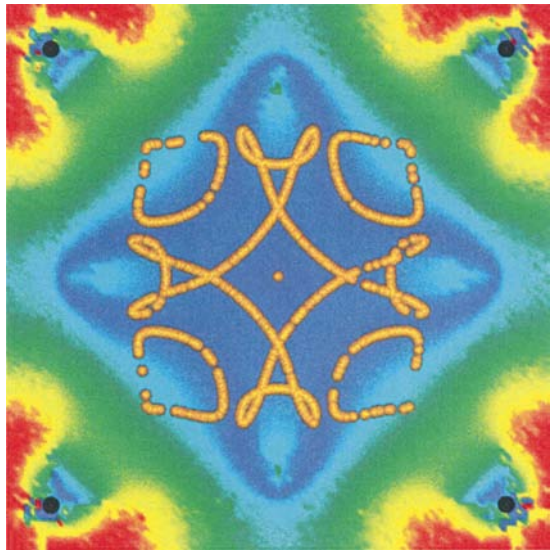

Figure 5
Electrostatic equilibrium of simultaneous Coulomb attraction and core repulsion for the ensemble of Fig. 4(*a*); the conjoint centroids (yellow) characterize force-free positions of the fragment inside the unit cell. For comparison, the pure Coulomb equilibrium is shown in the background.

$\mathcal{F} = \{X_1, \ldots, X_N\}$ and $\mathcal{P} = \{Y_1, \ldots, Y_M\}$ with $L = NM$ and equal weights $p_i = 1/L$,

$$R_{\mathcal{F}\times\mathcal{P}}(U) = (1/L)\sum_{i=1}^{L} \|Y_i - UX_i\|^2. \qquad (10)$$

For this residual, the centroid principle completely characterizes the (non-unique) best approximations of the sets $\mathcal{F}$ and $\mathcal{P}$, *i.e.* it provides a necessary and sufficient optimality condition.

3.3. Corollary 2 – sufficiency in case of Cartesian residual

Let the point sets $\mathcal{F}$ and $\mathcal{P}$ satisfy the assumptions of corollary 1, and let the Cartesian co-sets $\mathcal{F}_{\mathcal{F}\times\mathcal{P}}$ and $\mathcal{P}_{\mathcal{F}\times\mathcal{P}}$ have a common centroid

$$(1/L)\sum_{i=1}^{L} Y_i = (1/L)\sum_{i=1}^{L} X_i. \qquad (11)$$

Then, the residual $R_{\mathcal{F}\times\mathcal{P}}$ does not depend on orthogonal transformations U, *i.e.* the residual has a constant minimum value

$$R_{\mathcal{F}\times\mathcal{P}}(U) = (1/L)\sum_{i=1}^{L}\left(\|Y_i\|^2 + \|X_i\|^2\right)$$

and $U\mathcal{F} = (UX_1, \ldots, UX_N)$ is optimal for arbitrary rotations or roto-inversions U.

3.4. Proof

Without loss of generality, we may assume that both point sets $\mathcal{F}$ and $\mathcal{P}$ have been translated in such a way that the equi-weighted centroid of $\mathcal{F}$ is the origin $\mathcal{O}$ of the space $\Re^n$. Hence, for any orthogonal transformation U, we have

$$\mathcal{O} = U\mathcal{O} = U\left(\sum_{i=1}^{N}(1/N)X_i\right) = (1/N)\sum_{i=1}^{N} UX_i\,, \qquad (12)$$

where N is the number of points in $\mathcal{F}$.

According to theorem 2 (§2.5), it suffices to prove the identity [*cf.* equation (4)]

$$G(U) = (1/L)\sum_{k=i}^{L}\langle Y_k, UX_k\rangle \equiv 0.$$

Since $\mathcal{O}$ is orthogonal to any vector, particularly to the centroid of $\mathcal{P}$, we apply equation (12),

$$\begin{aligned} 0 &= \left\langle (1/M)\sum_{j=1}^{M} Y_j, \mathcal{O}\right\rangle \\ &= (1/MN)\left\langle \sum_{j=1}^{M} Y_j, \sum_{i=1}^{N} UX_i\right\rangle \\ &= (1/MN)\sum_{j=1}^{M}\sum_{i=1}^{N}\langle Y_j, UX_i\rangle \\ &= (1/L)\sum_{k=1}^{L}\langle Y_k, UX_k\rangle \\ &= G(U), \end{aligned}$$

with $L := MN$. The minimum value of the residual now follows from the expansion of

$$R_{\mathcal{F}\times\mathcal{P}} = (1/L)\|\mathcal{P}_{\mathcal{F}\times\mathcal{P}} - \mathcal{F}_{\mathcal{F}\times\mathcal{P}}\|^2$$

into its inner products [*cf.* equation (10)].

The corollary shows that, in general, uniqueness of the best approximations cannot be expected; the whole class of Cartesian (equi-weighted) residuals admits an infinite number of solutions that are optimal if and only if they share their centroid. For an illustration, the internet location http://www.hmi.de/people/maedler/ offers the link 'centroid principle': a fragment $\mathcal{F}^\star$ inside a point set $\mathcal{P}$ rotates through the minima of the Cartesian residual $R_{\mathcal{F}\times\mathcal{P}}$. In order to verify the principle, it was left to the minimizing evolution strategy to calculate the sequence of the centroid's positions $\overline{\mathcal{F}}_k \rightarrow \overline{\mathcal{F}^\star} = \overline{\mathcal{P}}$ during the approximation.

Among the relations $\rho \subseteq \mathcal{F}\times\mathcal{P}$, the Cartesian product $\rho = \mathcal{F}\times\mathcal{P}$ provides the most natural generalization of the centroid's minimum property from which we started in §2. As a matter of fact, a triangle spinning around its centroid is only a simple representative of the class of Cartesian residuals, which consists of point sets spinning around their conjoint centroid. In order to generalize the well known minimum property of the triangle, we have substituted the centroid of a point set by a second point set.

3.5. Example 2 – equi-weighted short-range solutions

Our second example is the class of short-range approximations, which may be of particular interest in practical applications. For this class, the spatial mesh $\rho \subset \mathcal{F}\times\mathcal{P}$ consists of the pairs (X_i, Y_j) of shortest distance, *i.e.*

$$(X_i, Y_j) \in \rho \text{ iff } \|X_i - Y_j\| = \min_{Y\in\mathcal{P}} \|X_i - Y\| \qquad (13)$$

for every $X_i \in \mathcal{F}$. Fig. 3 shows different short-range approximations of a triangle (white) inside a square (black). In Fig. 3(*a*), we want the short-range pairs

$$\rho = \left\{(X_1, Y_1), (X_2, Y_3), (X_3, Y_1)\right\}$$

to contribute to the residual; so we use the informed co-sets $\mathcal{F}_\rho := \mathcal{F}$ and $\mathcal{P}_\rho := (Y_1, Y_3, Y_1)$, and have to minimize the residual

$$R_\rho(U) = (1/3)\|\mathcal{P}_\rho - U\mathcal{F}\|^2.$$

The coloured background depicts Voronoi's cells for the four vertices of the square: for every point of the plane, the colour of the point indicates its distance to the nearest black vertex. Thus, the plane is partitioned into four ranges, and a pair (X_i, Y_j) contributes to the residual if both X_i and Y_j are in the same Voronoi cell. This may include the case of non-unique short-range pairs: in the best approximation depicted in Fig. 3(*c*), $X_2^\star$ lies on the border between two ranges; to achieve this solution, we have to use the co-sets $\mathcal{F}_\rho := (X_1, X_2, X_2, X_3)$ and $\mathcal{P}_\rho := \mathcal{P}$, and must minimize the value of

$$R_\rho(U) = (1/4)\|\mathcal{P} - U\mathcal{F}_\rho\|^2. \qquad (14)$$

Note that there is a way to compute at least some of the short-range solutions without specifying a spatial mesh ρ. If we use the (non-differentiable) residual

$$R(\mathcal{P}'; U) = \sum_{i=1}^{N} \min_{Y_i \in \mathcal{P}' \subset \mathcal{P}} \min_{U} \|Y_i - UX_i\|^2 \qquad (15)$$

and if the conjoint centroid is not fixed beforehand, the detection of the short-range partners Y_i is left to the optimization, and the algorithm can find best solutions like the ones shown in Figs. 3(*a*) and 3(*b*), but not the solution in Fig. 3(*c*). If we specify a conjoint centroid and minimize residual (15), the centroid principle provides a test on the validity of the computed result: it is a best approximation if and only if the detected co-sets have a conjoint centroid in accordance with corollary 1.

In order to demonstrate the effect of the centroid principle, we discuss below some simple examples, for which the best approximations can be predicted almost by eye.

In Fig. 3(*a*), each vertex of the white triangle enters the residual once, so the conjoint centroid $\mathcal{C}$ must be the usual centroid of the triangle (which divides the triangle's medians in the ratio of 1:2). Only the points Y_1 and Y_3 contribute to the short-range residual, the point Y_1 entering twice, so that the conjoint centroid $\mathcal{C}$ must divide the diagonal Y_1Y_3 of the square in the ratio of 1:2.

In Fig. 3(*b*), only the right-hand upper triangle of the black square is involved in the approximation, and the two triangles contribute with unique short-range pairs; according to the centroid principle the conjoint centroid $\mathcal{C}$ for the best approximation must be the usual centroid of the two triangles.

In Fig. 3(*c*), each of the vertices of the square contributes to the residual once, so the conjoint centroid $\mathcal{C}$ must be the centre of the square. Since one of the triangle's vertices, namely X_2, enters the residual twice, the conjoint centroid, in this case, is not the usual centroid of the triangle, but is shifted towards $X_2^\star$ and divides the horizontal median in the ratio of 1:1.

In order to verify the centroid principle, the location $\mathcal{C}$ of the conjoint centroid was not specified beforehand but was left to the optimization. Note how the symmetries of the square and of the isosceles triangle is mirrored in the optimal approximations. We may hope to derive a symmetry principle, in elementary geometric terms and as profound as the centroid principle, which could provide further characteristics of optimal solutions.

3.6. Example 3 – modelling of forces

It is an interesting task to invert the centroid principle and look for classes of weights that admit approximations of point sets $\mathcal{F}$ and $\mathcal{P}$ such that $\mathcal{F}$ and $\mathcal{P}$ exhibit a conjoint centroid. Such an inversion of the principle can be used, for instance, to model the force-free equilibrium orientations of a fragment $\mathcal{F}$ inside the unit cell $\mathcal{P}$ of an ionic crystal; at least in the sense of a first approximation that takes into account next-neighbour ions only.

For the sake of graphicness, we restrict ourselves to a simple fictitious ensemble consisting of a negative ion $\mathcal{F} = \{X_1^-, X_2^-\}$ inside a plane ionic counterpart $\mathcal{P} = \{Y_1^+, \ldots, Y_4^+\}$, which is kept fixed. Since we just want to demonstrate the underlying geometric principle, we neither consider infinity of the crystal nor any relaxations of the point charges, which are assumed to have magnitude $e = 1$. Also, charge balance is not requested, and force constants are used that fit with the size and dimension of the sets of ions in order to produce the equilibria we would like to visualize.

At first, only Coulomb interactions between all pairs (X_i, Y_j) are taken into account (*cf.* Fig. 4). This means that the forces $\mathcal{K}_{ij}$ between ions X_i and Y_j of opposite charge are of the form

$$\mathcal{K}_{ij}(X_i) = p'_{ij}(X_i - Y_j), \quad i = 1, 2, \quad j = 1, \ldots, 4,$$

with coefficients

$$p'_{ij}(X_i) := \|X_i - Y_j\|^{-3}.$$

After normalization, the interactions read

$$\mathcal{K}_{ij}(X_i) = \|X_i - Y_j\|^{-2}(X_i - Y_j)/\|X_i - Y_j\|,$$

which is Coulomb's law for our simplified situation.

In order to apply the centroid principle, we use the Cartesian co-sets of $\mathcal{F}$ and $\mathcal{P}$ for $\rho = \mathcal{F} \times \mathcal{P}$ [*cf.* equation (8)],

$$\mathcal{F}_\rho := (X_1, X_1, X_1, X_1, X_2, X_2, X_2, X_2)$$

and

$$\mathcal{P}_\rho := (Y_1, Y_2, Y_3, Y_4, Y_1, Y_2, Y_3, Y_4).$$

Then, after re-indexing, the resultant force can be written in the form

$$\mathcal{K}(\mathcal{F}) = \sum_{i=1}^{8} p'_i(X_i - Y_i).$$

For

$$s = s(\mathcal{F}) := \sum_{i=1}^{8} p'_i$$

and $p_i = p_i(\mathcal{F}) := p'_i/s$, we have $p_i > 0$, $\sum p_i = 1$, and the following equation holds:

$$\mathcal{K}(\mathcal{F}) = s \sum p_i(X_i - Y_i) = s(C_{\mathcal{F}_\rho} - C_{\mathcal{P}_\rho}), \qquad (16)$$

i.e. for fragment positions $\mathcal{F}$ with finite sums s the ions are in equilibrium position if and only if the weights $p_i = p'_i/s$ result in a conjoint centroid

$$C_{\mathcal{F}_\rho} = \sum p_i X_i = \sum p_i Y_i = C_{\mathcal{P}_\rho}.$$

In this sense, a conjoint centroid characterizes the Coulomb equilibria among the fragment orientations inside the unit cell of the crystal. Note that we have to take the centroids of the co-sets $\mathcal{F}_\rho$ and $\mathcal{P}_\rho$ in order to achieve this result.

In Fig. 4(*a*), the star-shaped dark-blue line and the centre indicate the conjoint centroids $C_{\mathcal{F}_\rho} = C_{\mathcal{P}_\rho}$ of the negatively charged dumbbell $\mathcal{F} = \{X_1, X_2\}$ of length 1 and the positively charged square $\mathcal{P} = \{Y_1, \ldots, Y_4\}$ of edge length 2. To compute the figure, for every point P of a 100×100 grid, we used an evolution strategy (see §4) in order to minimize the deviation of the centroids from P over the space of isometric mappings $\mathcal{F} = A + U(\mathcal{F}_0)$, where $\mathcal{F}_0$ is an initial position of the fragment,

$$d(\mathcal{F}^\star, P) = \min_{\mathcal{F}}\Big(\|C_{\mathcal{F}_\rho} - P\| + \|C_{\mathcal{P}_\rho} - P\|\Big).$$

We can express the resultant *via* the difference of the centroids and estimate the force on the optimal fragment

$$\begin{aligned}\|\mathcal{K}(\mathcal{F}^\star)\| &= s(\mathcal{F}^\star)\|C_{\mathcal{F}^\star_\rho} - C_{\mathcal{P}_\rho}\| \\ &\le s(\mathcal{F}^\star)\Big(\|C_{\mathcal{F}^\star_\rho} - P\| + \|C_{\mathcal{P}_\rho} - P\|\Big).\end{aligned}$$

Hence, a conjoint centroid $P = C_{\mathcal{F}_\rho} = C_{\mathcal{P}_\rho}$ indicates a resultant $\mathcal{K}(\mathcal{F}^\star) = \mathcal{O}$, and the iso-lines $d^\star(P) = 0$ (or the iso-surfaces in the spatial case) of the function

$$d^\star(P) := s(\mathcal{F}^\star)d(\mathcal{F}^\star, P)$$

represent the equilibrium states of $\mathcal{F}$ in $\mathcal{P}$, one of which is depicted in Fig. 4(*a*). Values $d^\star(P) > 0$ still give a qualitative impression of the force, at least in the sense that they provide an upper bound for the force on the fragment 'near' the points P.

Additionally, a combined Monte Carlo and evolution method was used for Fig. 4(*b*) in order to compute the conjoint centroids: at each Monte Carlo step, the fragment $\mathcal{F}_0$ is randomly 'thrown' into the cell; then a local minimization finds positions with identical centroids, thus covering the iso-lines $d^\star(P) = 0$ more or less completely. In order to demonstrate the sensitive dependence of the conjoint centroid on a symmetric configuration, the quadrangle is slightly distorted along the diagonals [compared with the square in Fig. 4(*a*) by about 2 and 5% in the left-hand and right-hand upper vertices, respectively].

In essence, the same method can be applied when repulsion of the atom cores is added. To achieve the simultaneous effects of Coulomb attraction and core repulsion as depicted in Fig. 5, these forces are modelled (for this fictitious example) by means of the coefficients

$$p_i'(X_i) := \|X_i - Y_i\|^{-3}(1 - B\|X_i - Y_i\|^{-5}).$$

For comparison, the proportionality constant is $B = 0.15$ for the conjoint centroids and $B = 0$ for the Coulomb background. In order to meet the assumptions of the centroid principle, only fragment positions $\mathcal{F}_\rho$ with positive coefficients $p_i'(X_i) > 0$ are admitted for minimization.

This simple example illustrates the basic idea of how to invert the centroid principle in order to model forces: if the weights can be used to express the force laws, the resultant is the difference vector of the weighted centroids of the interacting partners [up to a scalar function $s(\mathcal{F})$, *cf.* equation (16)], and every conjoint centroid will characterize an equilibrium state. A forthcoming publication will present more details, together with a crystallographic application that demands a more realistic treatment of the forces involved.

For the crystallographic problems in §5, we return to 'forward applications' of the principle, in order to achieve results that are more qualitative in the sense that they are based on geometric concepts only. Before we go into more detail, some computational aspects are discussed; we feel that

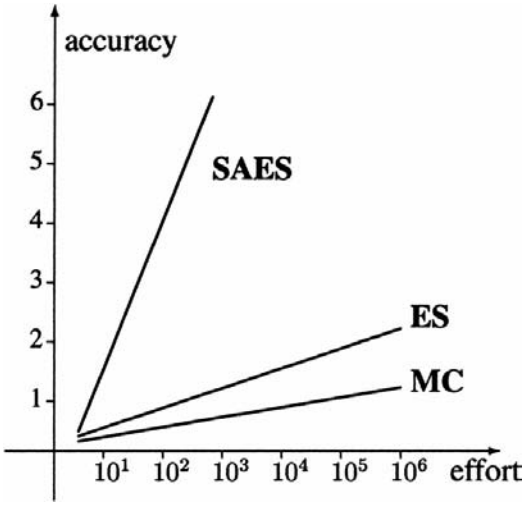

Figure 6
A qualitative comparison of the basic versions of Monte Carlo methods (MC), evolution strategies (ES) and self-adapting evolution strategies (SAES). The lines depict the averaged ratio of accuracy (number of valid decimals in the solution) over effort (number of trials or generations on a logarithmic scale).

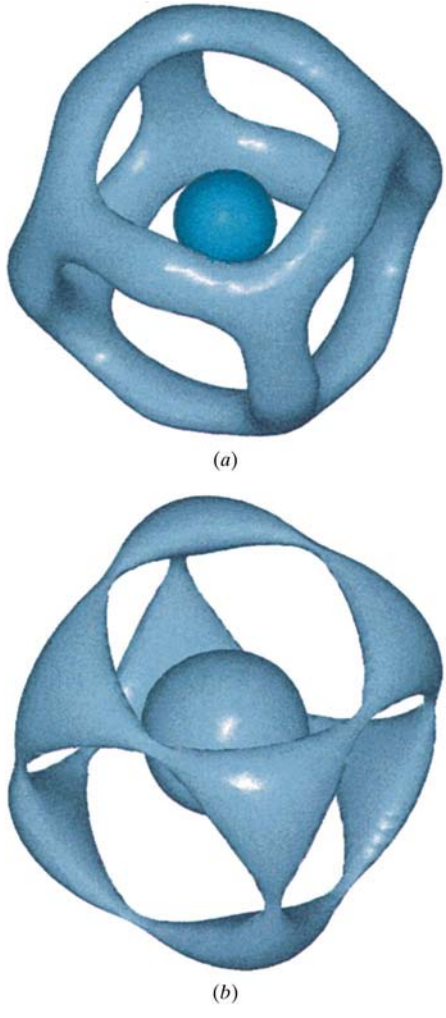

Figure 7
Equi-electron density surfaces of cubic KPF_6 at ambient conditions (*a*) and at a pressure of 0.15 GPa (*b*).

we should not release the centroid principle without suggesting a flexible computation method that is able to exploit the expressive modelling power of the principle, thus making it available for practical applications.

4. Computational aspects

Monte Carlo methods (MC) and evolution strategies (ES) in particular exhibit several advantageous properties that can compensate for their possibly low convergence rates and make these methods a useful computation tool. They are not sensitive to phenomena like ill-conditionedness of the optimal transformations, and they cope with non-unique solutions: at least statistically they tend towards completeness of the solution set; this is an inevitable requirement, for instance, if structural fragments are to be computed in full disorder, in order to explain a spatial or a space-and-time average of a physical entity observed in experiments (see also §5). Last, but not least, self-adapting evolution strategies (SAES) (*i.e.* Bäck, 1998) are able to provide high accuracy in their results. This can be essential for crystallographic applications (like, for instance, for the case of KPF_6 in §5): if symmetry is involved, and if the calculations are performed on normalized scales, the solutions may show exact fractions, which a computer program should indicate through high accuracy.

In this section, we compare the basic algorithms of MC, ES and SAES with respect to the relation of accuracy and effort. For each method, the short-range residual [*cf.* equation (15) of example 2 in the preceding section]

$$R(\mathcal{P}'; U) = \min_{Y_i \in \mathcal{P}' \subset \mathcal{P}} \min_{U} \sum_{i=1}^{6} \|Y_i - UX_i\|^2$$

is used to compute the minimum rotation $U^\star$ of a regular octahedron $\mathcal{F} = \{X_1, \ldots, X_6\}$ in a fixed cube $\mathcal{P} = \{Y_1, \ldots, Y_8\}$. The determination of the optimal subset $\mathcal{P}' \subset \mathcal{P}$ of cube vertices $Y_i \in \mathcal{P}'$ is part of the problem, which becomes non-differentiable this way. The conjoint centroid is the origin $\mathcal{O}$; the edge of the cube has the length 2 and is equal to the total height of the octahedron. ES and SAES computations start from an octahedron whose axes coincide with the coordinate system. We use this example for the sake of graphicness only; according to our experiences in rather different applications, Fig. 6 gives a reliable qualitative comparison of the three methods and of their ratios of accuracy *versus* effort. Here, effort is measured by the number of trials in MC and by the number of generations in ES and SAES, while accuracy is the number of valid decimal places in the solutions $X_i^\star$, which, in this example, are signed permutations of the point (x, x, z) with $x = 2/3$ and $z = 1/3$.

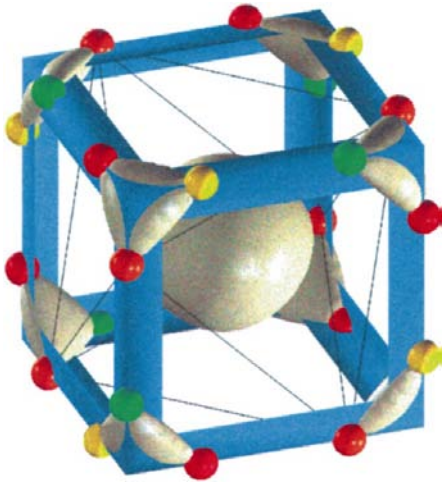

Figure 8
High-pressure configurations of cubic KPF_6 at 0.15 GPa.

4.1. Monte Carlo method (MC)

In its purest version, MC successively generates objects at random (*e.g.* orthogonal matrices U) and keeps the best with respect to an objective function [*e.g.* the function $G(U)$, see equation (4)]. The method is 'blind' in the sense that it neither

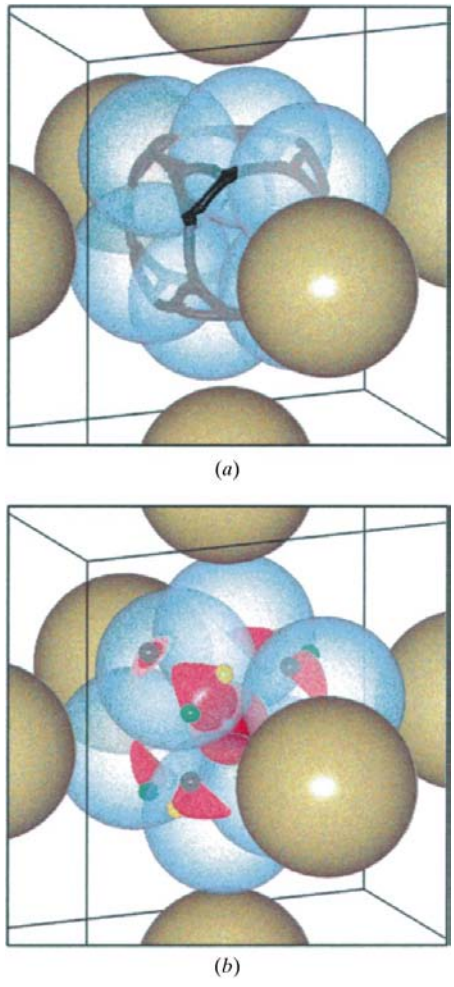

Figure 9
Pressure-dependence of disorder in KPF_6 as predicted in a qualitative model. (*a*) At ambient pressure, a static disorder of six stable PF_6 orientations could co-exist with a dynamic disorder of superposed PF_6 trajectories close to the black 'evolution tracks'. (*b*) At a pressure of 0.15 GPa, the disorder is reduced to four stable high-pressure orientations.

exploits any knowledge about the search space nor uses any heuristic information. Nevertheless, if the problem is of 'moderate magnitude' [like the search space of the orthogonal transformations $U = U(\theta_1, \theta_2, \theta_3)$ which are generated by three independent rotation angles], the method will find first approximations of optimal objects in acceptable time. In general, high accuracy of the solutions cannot be expected from MC; note that the effort axis in Fig. 6 is logarithmic. On average, more than one to two valid decimal places were not found for our example; in particular, the results did not indicate the fractions.

4.2. Evolution strategy (ES)

Evolutionary algorithms imitate mechanisms of the biological evolution in order to optimize an ancestor object (*e.g.* the starting position of the above octahedron) along a sequence of improved offspring. In its most simple form, for every generation ES generates a child by random mutations of the parent's parameters (*e.g.* a new position for the parent octahedron) and compares the fitness values of the two; the fitter one [the position with the higher G value in equation (4)] becomes the parent for the next generation. The random mutation is taken, for instance, from a normal distribution; the width of the distributions is 'tuned' to the problem at the outset and is then kept constant during the evolution.

ES uses heuristic knowledge of the kind 'if an increase in the fitness is shown for a set of parameters, there may be higher increase near those parameters'. Of course, this is 'just heuristics' and may fail at particular evolution steps, but for many problems this knowledge enables ES to produce better convergence rates than MC. As a consequence, about three valid decimal places can be expected at an averaged effort of a million generations, which, in our example, already suggests the possibility of fractions in the solution.

4.3. Self-adapting evolution strategy (SAES)

The smaller the width of the random distribution, the smaller the preferred random mutations. Obviously, this observation provides a simple control of evolutionary success: SAES observes its success rate and uses additional heuristic knowledge of the kind 'if success turns rare, the mutations may be too large'. Lowering the width of the distribution (*i.e.* preferring smaller angles $\theta_1, \theta_2, \theta_3$ for the rotations of the parent octahedra) is a simple but powerful mechanism of self-adaptation in evolutionary programs. In Knorr & Mädler (1999), we used appropriate variants of an elementary evolution scheme in order to treat various aspects of crystal disorder. In all these applications, SAES provided accurate solutions at reasonable effort. For the example at hand, the SAES line in Fig. 6 shows that the fractions are computed to up to six decimal places at an average of less than 1000 generations.

5. Applications of the centroid principle

Although the centroid principle had not been proved at that time, all applications in Knorr & Mädler (1999) did benefit from the principle in one way or the other. Many of the optimizations were performed with free centroids, so that the conjoint centroid proved to be a plausible and qualitatively justified assumption, which was observed 'in action' and which helped to understand various aspects of disorder in different compounds, such as tetrahydrofuran in the $[5^{12}6^4]$-cage of ZMS-39, 1,3-dioxolanesilicasodalite and cubic KPF_6. Now that the principle has been proved and is better understood, qualitative explanations of the observed disorders can be given; up to a certain degree, we are able to predict some of the phenomena on the basis of a qualitative model.

In this section, we will demonstrate how the centroid principle was successfully used to answer questions concerning the pressure-dependent static or dynamic disorder of KPF_6. Our answers include (i) the computation of its disordered set of high-pressure conformations from diffraction data, (ii) the prediction of these conformations through a qualitative model, (iii) the reproduction of these conformations as solutions to a virtual high-pressure experiment performed in a qualitative model, and (iv) the computation of a disordered set of possible reorientation paths, which qualitatively explains the shape of the electron-density distribution reconstructed from a diffraction experiment at ambient pressure.

The main reason for calling our model qualitative is the fact that it is based on geometry only and has not incorporated any higher quantitative concepts from physics. For instance, the virtual high-pressure experiment (iii) is performed without any quantitative notion of force, pressure *etc.* Nevertheless, it results exactly in the disordered solutions as computed from the diffraction data of the real experiment (i); this shows that qualitative can be exact. Of course, it can also mean approximate, as, for instance, in the case of the suggested dynamic disorder of KPF_6 at ambient pressure (iv).

Recently, Sowa, Knorr *et al.* (1999) studied the spatial electron-density distribution in cubic KPF_6 as a function of pressure. These electron densities were reconstructed from X-ray single-crystal diffraction data by means of a maximum-entropy method. Fig. 7 depicts two of the equi-density surfaces at ambient conditions (Fig. 7*a*) and at high pressure (Fig. 7*b*).

(i) At 0.15 GPa, the electron density exhibits a set of eight maxima $\mathcal{P} = \{M_1, \ldots, M_8\}$ in the form of a regular cube which is concentric with the surface in Fig. 7(*b*) and whose vertices M_j lie inside the eight triangular cushion-like parts of the surface. Of course, the density maxima must be caused by a disorder of PF_6^- octahedra $\mathcal{F} = \{F_1, \ldots, F_6\}$ with unknown orientations inside the equi-density surface. So the question is, how do the PF_6^- anions, with their six ions F_i^-, superpose in a spatial average in order to produce the eight vertices M_j of the cube $\mathcal{P}$?

If we assume that the disordered F ions are as close as possible to the density maxima to which they contribute with their electrons, we have identified a geometric approximation problem: compute orientations for the octahedron $\mathcal{F}$ whose

vertices F_i are as close as possible to suitable subsets of the cube vertices M_j.

The sphere in the centre of the equi-surface in Fig. 7(*b*) belongs to the P atom and seems to indicate a concentric position of the cube and the disordered octahedra. Thus, as a first try, we assume a conjoint centroid for the cube $\mathcal{P}$ and the octahedra $\mathcal{F}$ and minimize the short-range residual from equations (13) or (15),

$$R(\mathcal{P}'; U) = \sum_{i=1}^{6} \min_{M_i \in \mathcal{P}' \subset \mathcal{P}} \min_{U} \|M_i - UF_i\|^2.$$

After a few restarts, the SAES algorithm finds four different octahedra $\mathcal{F}_k$. All computations are performed on normalized scales with the PF bondlength $l = 1$. We need three non-collinear points to describe the solutions: the conjoint centroid of $\mathcal{F}_k$ and $\mathcal{P}$ is at the origin $\mathcal{O}$. Two further points for $\mathcal{F}_1$, for instance, are

$$\begin{aligned} X_{1,1} &= (x, x, z) \\ X_{1,2} &= (x, -z, -x) \end{aligned} \qquad (17)$$

with $x = 2/3$ and $z = 1/3$. All other vertices in the disorder $\mathcal{F}_1, \ldots, \mathcal{F}_4$ are signed permutations of $X_{1,1}$ (like $X_{1,2}$). The computations include the check for compatible ionic radii as well as the test that the centroid principle holds for every pair $(\mathcal{F}_k, \mathcal{P}')$. The optimal orientations $\mathcal{F}_k$ are depicted in Fig. 8 in different colours. Every octahedron approximates a different subset $\mathcal{P}' \subset \mathcal{P}$ of six of the density maxima M_j. The vertices of the solutions $\mathcal{F}_k$ lie on edges of the blue cube, which is concentric and parallel to $\mathcal{P}$. Always, three F anions of different PF_6^- octahedra are close to one density maximum M_j amongst them; in fact, M_j is the centroid of its three anions in good agreement with the coordinates of M_j as derived from the experiment data. This is a possible explanation of the cushion-like forms that make up the shape of the density in Fig. 7(*b*).

(ii) In this way, we have determined the disorder from the maxima of the electron density that was reconstructed from experiment data. There is, however, another method to derive this disorder; it is predictive in the sense that it does not refer to experiments but is based on a qualitative model. Our assumption now is that the disordered PF_6^- fragments are stretched in a frame of its six nearest K^+ ions. Note that, in Fig. 8, all F anions of the four octahedra are on the edges of the blue cube. From the coordinates of the density maxima, we know that the K cations are located on the centred normals of the six faces of this cube; *i.e.* in the solutions $\mathcal{F}_k$ every F anion is in best approximation with two different K cations (not shown in Fig. 8). Table 1 represents geometric expert knowledge for a suitable spatial mesh ρ of an octahedron inside an octahedral environment. If we arrange the pairs (F_i, K_j) in the linear order (8) of §3 and select the informed co-sets

$$\mathcal{F}_\rho := (F_1, F_1, F_2, F_2, \ldots, F_6, F_6)$$

for the set of F anions $\mathcal{F} = \{F_1, \ldots, F_6\}$ and

$$\mathcal{P}_\rho := (K_1, K_4, K_2, K_3, K_3, K_5, K_4, K_6, K_5, K_2, K_6, K_1)$$

Table 1
Specification of a spatial mesh ρ for the PF_6 fragment $\mathcal{F}$ and the set $\mathcal{P}$ of its K^+ neighbours.

In the minimization residual R_ρ every F anion is supposed to interact with two K cations.

Anion	Partner cations
F_1	K_1, K_4
F_2	K_2, K_3
F_3	K_3, K_5
F_4	K_4, K_6
F_5	K_5, K_2
F_6	K_6, K_1

for the set $\mathcal{P} = \{K_1, K_2, \ldots, K_6\}$ of K cations, we have identified the first of four equi-weighted residuals,

$$R_{\rho_1}(U) = \|\mathcal{P}_{\rho_1} - U\mathcal{F}_{\rho_1}\|^2 = \sum_{i=1}^{12} \|K_i - UF_i\|^2,$$

which we can minimize, starting with random orientations for $\mathcal{F}$. For symmetry reasons (*cf.* Fig. 8), there exist three further residuals $R_{\rho_2}, R_{\rho_3}, R_{\rho_4}$ of the same kind. Remarkably enough, the minimization of the four residuals perfectly reproduces the disorder $\mathcal{F}_1, \ldots, \mathcal{F}_4$ which was derived by numerical evaluation of the diffraction data in (i).

Note that this alternative derivation of the disorder reveals certain predictive capabilities of our qualitative model: some geometric analysis of the PF_6^- octahedron $\mathcal{F}$ inside its octahedral K^+ environment $\mathcal{P}$ yields hypothetical approximation residuals R_ρ whose minima might be stable orientations of the fragment. At this point, the model uses crystallographic expertise in order to decide, for instance, whether the ionic radii are compatible for a predicted orientation of $\mathcal{F}$ in $\mathcal{P}$. This, for example, is not the case for the fully ordered KPF_6 solution to the residual $R_\rho(U) = \|\mathcal{P} - U\mathcal{F}\|^2$, where the two octahedra have a conjoint centroid and coincident axes. On the other hand, the model predicts a compatible static disorder for KPF_6 at ambient conditions which could co-exist with a dynamic disorder of the fragment [see (iv) below].

Is there a way to relate this KPF_6 disorder qualitatively to high pressure in a plausible sense?

(iii) Our assumption here is that we do not need to know force or pressure quantitatively in order to predict a fragment's behaviour inside a crystal which is being squeezed under the condition that symmetry is not broken. Up to a certain degree it may suffice to model this process and its result by the fragment's spatial answer to pressure, which is to sidestep or to give way in its narrowing environment. In this way, we ran a virtual high-pressure experiment: an SAES algorithm maximizes the fragment's distances from a surrounding cube which is concentric with the blue cube in Fig. 8 (but larger) and which qualitatively represents the cubic crystal (Knorr & Mädler, 1999). Amazingly enough, this computer simulation, although based on a rather coarse model of pressure, exactly reproduces the above high-pressure configurations $\mathcal{F}_1, \ldots, \mathcal{F}_4$. Therefore, with respect to the space available for the PF_6 anion, the structure of KPF_6,

experimentally observed at 0.15 GPa, is already the most compressible formation in space group $Fm\bar{3}m$. Indeed, Sowa, Ahsbahs & Kutoglu (1999) show that a further increase of the pressure triggers a phase transition into a rhombohedrally distorted CsCl-like structure. So virtual experiments of this kind may be helpful to predict phase transitions in disordered structures, at least qualitatively.

Note that the disorder $\mathcal{F}_1, \ldots, \mathcal{F}_4$ [*cf.* equation (17)] equals the solutions to the approximation problem that we used as a benchmark in §4. In fact, if we compute the disorder on normalized scales with the vertices of the octahedron at distance 1 from its centre, our model predicts that the solutions are independent of the size of the host octahedron, and that, if the ionic radii are compatible, the most compressible but still stable orientations of the fragment $\mathcal{F}$ in space group $Fm\bar{3}m$ will conjointly produce eight maxima M_j of the electron-density distribution in the form of the vertices of a cube, which are located at $M_1 = (5/9, 5/9, 5/9)$ and its seven symmetric equivalents. Up to the resolution limits of the KPF_6 high-pressure experiment, this prediction is in accordance with the density maxima as numerically evaluated from the reconstructed electron density. This may be seen as a mutual confirmation of the real experiment and its model-based qualitative simulation. Of course, the model cannot tell the maximum value of the density, only its locations.

(iv) Under ambient conditions, the reconstructed electron-density distribution exhibits 12 maxima that are located at the midpoints of the 12 edges of the cube-like equi-density surface in Fig. 7(*a*). Because of symmetry, we can build six different residuals

$$R_{\tau_k}(U) = \|\mathcal{P}_{\tau_k} - U\mathcal{F}_{\tau_k}\|^2, \quad k = 1, \ldots, 6,$$

with informed co-sets $\mathcal{F}_{\tau_k}$ and $\mathcal{P}_{\tau_k}$, for instance,

$$\mathcal{F}_{\tau_1} := (F_1, F_1, F_2, F_2, F_3, F_4, F_5, F_6)$$

and

$$\mathcal{P}_{\tau_1} := (K_1, K_6, K_2, K_5, K_3, K_4, K_3, K_4).$$

The minimization of these residuals reveals the possibility of stable orientations of PF_6^- inside its K^+ host, with two opposite vertices at the midpoints of opposite edges of a suitable cube and the other four vertices pairwise on the diagonals of opposite faces of the cube. These solutions cannot be derived numerically from the experiment data, which do not show any density maxima somewhat near to the four F^- ions on the diagonals. So the prediction of the stable disorder $\mathcal{F}_1, \ldots, \mathcal{F}_6$ can hardly be the full explanation of the shape of the electron density, but it contributes to the discussion of the conspicuous middle parts of the edges in Fig. 7(*a*).

According to the structured version of the centroid principle (see corollary 1; §3.1), the conjoint centroid of the co-sets $\mathcal{F}_{\tau_k}$ and $\mathcal{P}_{\tau_k}$, $k = 1, \ldots, 6$, is the centre of the P atom, which, in this case, is also the conjoint centroid of the six stable orientations $\mathcal{F}_k$ and the octahedral K^+ host. In Knorr & Mädler (1999), we qualitatively investigated the spatial aspects of a possibly dynamic disorder in a purely geometric way: the conjoint centroid is fixed to the centre of an interaction polyhedron, which for this cubic crystal is a cube whose faces are tangent to the six nearest K^+ neighbours at an ionic radius of 1.38 Å. The influence of the electric field is modelled by restraining the fragment's mobility to rotations around the conjoint centroid that stay inside the cube. Then automorphic images $\mathcal{F}'_k$ of the stable orientations $\mathcal{F}_k$ (in particular C_3 rotations around an axis through the midsts of opposite faces of the fragment and C_4 rotations around its longitudinal axes) are used as goals for an evolution strategy that minimizes the overall distance of the first ancestor $\mathcal{F}_k$ from its image $\mathcal{F}'_k$. In this way, the PF_6 octahedron is driven through the space remaining inside the crystal, and the tracks of its F vertices indicate the space for reorientation pathways for the fragment. As a result, the tracks superpose to the closed black trajectory in Fig. 9(*a*), which passes through all of the stable orientations $\mathcal{F}_1, \ldots, \mathcal{F}_6$ and which perfectly fits and explains the shape of the electron-density distribution of Fig. 7(*a*). In this sense, our qualitative model suggests the coexistence of stable orientations and dynamic behaviour of the fragment in order to explain the disorder observed under ambient conditions, while, at a pressure of 0.15 GPa, this disorder is reduced to the four stable high-pressure formations shown in Fig. 9(*b*), only one of which (the blue one) is depicted with a realistic ratio of magnitude in its ionic radius.

6. Summary and conclusions

We have proved a useful geometric centroid principle for rigid point sets: in order that two such sets achieve a best approximation, they must conjoin their centroids. To derive a more elaborate version of the principle that better meets the demands of practical applications, we introduced informed co-sets and co-set residuals; these concepts can be used to specify desirable spatial meshings among the point sets approximating each other.

The principle of the conjoint centroid is of fourfold importance: (i) it describes a fundamental geometric property of the Euclidean space; (ii) it provides a flexible concept of approximation for rigid point sets and a necessary condition for their optimal approximation; (iii) its inversion can be used to model forces; and (iv) it is a fundamental building block for qualitative models of physical problems which are, in essence, of geometric nature and which can be reduced to geometric approximation problems. The embedding of a disordered structural fragment into the maxima or other conspicuous point sets of its electron-density distribution is but one example; other crystallographic applications are the (exact) prediction of pressure-dependent static disorders and the (approximate) computation of possible reorientation pathways by means of an evolution strategy. This is our suggestion of a qualitative model for disorder in crystals: represent the disorder implicitly in the form of minima of suitably selected co-set residuals and solve these approximation tasks by self-adapting evolution strategies using chemical expertise to reject solutions with incompatible potentials; up to a certain

degree, such a computer-based model can compensate for the lack of explicit formulae.

References

Bäck, T. (1996). *Evolutionary Algorithms in Theory and Practice.* Oxford University Press.

Bäck, T. (1998). *Fundam. Inf.* **35**, 51–66.

Giacovazzo, C. (1994). *Fundamentals of Crystallography*, edited by C. Giacovazzo, pp. 61–140. Oxford University Press.

Knorr, K. & Mädler, F. (1999). *J. Appl. Cryst.* **32**, 902–910.

Knorr, K., Mädler, F. & Papoular, R. J. (1998). *Microporous Mesoporous Mater.* **21**, 353–363.

Sowa, H., Ahsbahs, H. & Kutoglu, G. (1999). *Z. Kristallogr.* **214**, 751–757.

Sowa, H., Knorr, K., Mädler, F., Ahsbahs, H. & Kutoglu, G. (1999). *Z. Kristallogr.* **214**, 542–546.

Valenza, R. (1993). *Linear Algebra – An Introduction to Abstract Mathematics.* Berlin: Springer-Verlag.

Weisstein, E. W. (1999). *CRC Concise Encyclopedia of Mathematics.* Boca Raton, Florida: CRC Press.